

Determination of charge transport activation energy and injection barrier in organic semiconductor devices

S. Züfle, S. Altazin, A. Hofmann, L. Jäger, M. T. Neukom, W. Brütting, and B. Ruhstaller

Citation: *Journal of Applied Physics* **122**, 115502 (2017); doi: 10.1063/1.4992041

View online: <https://doi.org/10.1063/1.4992041>

View Table of Contents: <http://aip.scitation.org/toc/jap/122/11>

Published by the [American Institute of Physics](#)

Articles you may be interested in

[The use of charge extraction by linearly increasing voltage in polar organic light-emitting diodes](#)
Journal of Applied Physics **121**, 175501 (2017); 10.1063/1.4982903

[Organic electroluminescent diodes](#)
Applied Physics Letters **51**, 913 (1987); 10.1063/1.98799

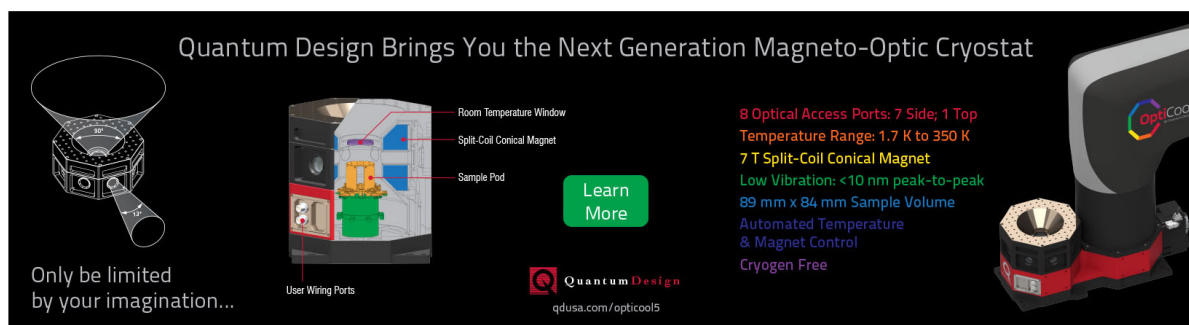
[Electron and hole transport in the organic small molecule \$\alpha\$ -NPD](#)
Applied Physics Letters **110**, 073301 (2017); 10.1063/1.4976205

[Mobility balance in the light-emitting layer governs the polaron accumulation and operational stability of organic light-emitting diodes](#)
Applied Physics Letters **111**, 203301 (2017); 10.1063/1.5004623

[An improved method for extraction of mobility from space charge limited current in organic semiconductor films](#)
Journal of Applied Physics **121**, 155501 (2017); 10.1063/1.4981242

[High-resolution charge carrier mobility mapping of heterogeneous organic semiconductors](#)
Applied Physics Letters **111**, 083302 (2017); 10.1063/1.4999762

Quantum Design Brings You the Next Generation Magneto-Optic Cryostat



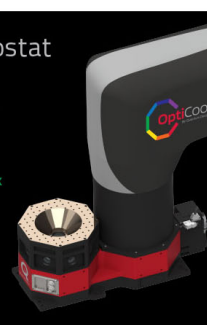
Only be limited by your imagination...

Room Temperature Window
Split-Coil Conical Magnet
Sample Pod
User Wiring Ports

Learn More

Quantum Design
qdusa.com/opticool5

8 Optical Access Ports: 7 Side; 1 Top
Temperature Range: 1.7 K to 350 K
7 T Split-Coil Conical Magnet
Low Vibration: <10 nm peak-to-peak
89 mm x 84 mm Sample Volume
Automated Temperature & Magnet Control
Cryogen Free



Determination of charge transport activation energy and injection barrier in organic semiconductor devices

S. Züfle,^{1,2,a)} S. Altazin,² A. Hofmann,³ L. Jäger,³ M. T. Neukom,^{1,2} W. Brütting,³ and B. Ruhstaller^{1,2}

¹*Institute of Computational Physics, Zurich University of Applied Sciences, Technikumstr. 9, 8401 Winterthur, Switzerland*

²*Fluxim AG, Technoparkstr. 2, 8406 Winterthur, Switzerland*

³*Institute of Physics, University of Augsburg, 86135 Augsburg, Germany*

(Received 26 June 2017; accepted 15 August 2017; published online 19 September 2017)

Charge carrier transport in organic semiconductor devices is thermally activated with characteristic activation energies in the range of 0.2–0.6 eV, leading to strongly temperature-dependent behaviour. For designing efficient organic semiconductor materials and devices, it is therefore indispensable to understand the origin of these activation energies. We propose that in bilayer organic light-emitting diodes (OLEDs) employing a polar electron transport layer, as well as in metal-insulator-semiconductor (MIS) devices, the hole injection barrier E_{inj} and the hole mobility activation energy E_{μ} can be decoupled from each other if temperature-dependent capacitance-frequency (C-f-T) and MIS-CELIV (charge extraction by linearly increasing voltage) experiments are combined. While the C-f-T signal contains information of both injection and transport, the CELIV current is expected to be insensitive to the electrode injection properties. We employ numerical drift-diffusion simulations to investigate the accuracy of this analytical parameter extraction approach and to develop criteria for its validity. We show that the implicit assumption of constant charge density and field profiles leads to systematic errors in determining the activation energies. Thus, one should be aware of the intrinsic limitations of the analytical Arrhenius fit, and for more accurate parameter determination a full drift-diffusion modelling is advised. Applying the analytical method to a standard bilayer OLED, we find that the total activation energy of 0.5 eV for the hole current can be split into contributions of ≈ 0.25 eV each for injection barrier and mobility. Finally, we also discuss the broader applicability of this method for other device stacks and material combinations. © 2017 Author(s). All article content, except where otherwise noted, is licensed under a Creative Commons Attribution (CC BY) license (<http://creativecommons.org/licenses/by/4.0/>). [<http://dx.doi.org/10.1063/1.4992041>]

I. INTRODUCTION

There is great interest in the knowledge of the temperature-dependent behaviour of organic semiconductor materials and devices such as organic light-emitting diodes (OLEDs) and organic solar cells (OSCs). The reason for this is the operation temperature of such devices which is usually higher than room temperature. In OLEDs, Joule heating by the charge current leads to selfheating effects and an increase of the device temperature up to 70 °C.^{1–4} Conversely, in OSCs, parasitic absorption as well as nonradiative recombination also leads to operation temperatures in a similar range. However, many materials for these devices are usually still investigated under standard test conditions, which is 25 °C. Furthermore for OSCs, a standard illumination intensity and spectrum of 1 sun (AM1.5g) is employed for efficiency measurements.⁵ In contrast to this during real outdoor operation, solar cells will experience strongly changing temperatures due to daily cycling, sunlight incidence angle, and weather conditions like clouds or wind.^{6,7} In OLEDs used in display applications, the stack temperature may also change quickly; furthermore, different driving currents in different

pixels can lead to inhomogeneous two-dimensional temperature distributions. All these arguments show that it is indispensable to investigate the temperature dependence of charge transport in organic semiconductor materials and devices.

In OLEDs, good charge carrier injection is important to achieve high efficiencies. However, in standard devices it is challenging to distinguish effects of injection and transport, which in turn makes it difficult to characterize the energetic barrier for charge injection. Furthermore, the bipolar current depends on both electron and hole injection barriers as well as their mobilities, making the analysis rather challenging.

In this work, we present an approach to decouple the contributions of the hole injection barrier and the hole mobility activation energy in polar OLEDs.^{8,9} After introducing a simple equivalent circuit model, we propose a combination of two experiments to determine both activation energies. We then examine this hypothesis by means of numerical drift-diffusion simulation and investigate the accuracy of the extracted parameters. In Sec. V, we show that the presented method is also valid for metal-insulator-semiconductor (MIS) devices and can be generally applied to investigate new materials.

^{a)}Electronic mail: simon.zuefle@zhaw.ch

II. METHODS

For the study presented here, we concentrate on the temperature dependence of bilayer OLEDs employing a polar electron transport layer (ETL) [see Fig. 1(a)]. The devices with an active area of 0.036 mm^2 have been fabricated at Augsburg University using standard procedures that have already been described elsewhere.¹⁰ The layer stack is ITO/PEDOT:PSS/ α -NPD/Alq₃/Ca/Al. Hereby, ITO stands for the transparent conductive indium tin oxide electrode, PEDOT:PSS for the hole injection layer (HIL) poly(3,4-ethylenedioxythiophene) polystyrene sulfonate, α -NPD for the hole transport layer (HTL) N,N'-diphenyl-N,N'-bis(1-naphthyl)-1,1'-biphenyl-4,4'-diamine, and Alq₃ for the polar ETL Tris-(8-hydroxyquinoline)aluminum. Due to the misalignment of the energy levels, a hole injection barrier from PEDOT:PSS into α -NPD as depicted in Fig. 1(a) is assumed.^{11,12} The devices were encapsulated with a cover glass using epoxy. The active layer thicknesses are obtained from capacitance measurements.

We have performed capacitance-frequency and MIS-CELIV (which stands for metal-insulator-semiconductor, charge extraction by linearly increasing voltage) experiments with the all-in-one characterization platform Paios by Fluxim AG, Switzerland.¹³ The capacitance-frequency signal is the output of impedance spectroscopy, where at a given working point a small modulating voltage $V_{ac} = V_1 \cdot \sin(2\pi ft)$ with frequency f and amplitude $V_1 = 70 \text{ mV}$ is applied. The complex admittance Y , conductance G , and capacitance C are then evaluated using the resulting modulated current: $Y = I_{ac}/V_{ac} = G + i2\pi fC$. In the CELIV technique, a negative voltage ramp (or triangular voltage pulse) is applied to the device, leading to a constant displacement current (see also the [supplementary material](#)). If mobile charge carriers are present, they are extracted by the reverse field and lead to an additional current peak. The transient position of this peak can be related to the carrier drift mobility.^{14,15} For cooling, we employed the low-temperature module of Paios, which uses a cryostat chamber cooled by liquid nitrogen. The whole temperature sweep with intermittent capacitance-frequency (C-f-T) and MIS-CELIV acquisition is automated in the Paios software and can be performed within 2h, preventing

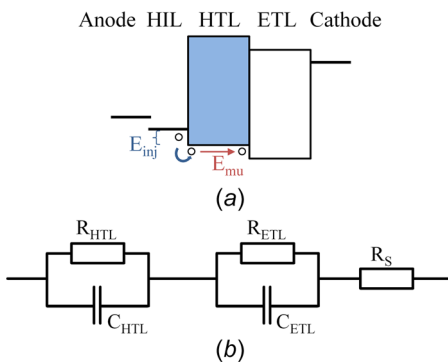


FIG. 1. Schematics of the bilayer OLED stack. (a) Energy levels and definition of the activation energies for hole injection and transport. (b) Equivalent circuit representation as a series of two RC-circuits and a series resistance.

accidental degradation of the device. The device temperature is logged using a PT100 temperature sensor which is placed on the glass substrate of the sample. For enhanced signal quality, the CELIV measurements were performed 5 times and then averaged.

For the second part of this work, we used the commercial drift-diffusion simulation software Setfos which is able to simulate both the (large-signal) transient CELIV experiment and the (small-signal) capacitance-frequency method with the same set of model parameters.¹⁶ The drift-diffusion approach is often employed to describe charge transport processes in organic electronics, where carriers can either drift in the electric field or diffuse due to charge density gradients. In previous publications, we have already demonstrated the possibility of modelling polar ETLs in bilayer OLEDs in the steady-state and frequency domain with Setfos.^{15,17}

III. EXPERIMENTAL RESULTS AND ANALYTICAL MODEL

In polar bilayer OLEDs, hole injection into the hole transport layer occurs already below the built-in voltage (V_{bi} , being the difference in electrode work functions) due to the permanent polarization of the electron transport layer Alq₃, owing to spontaneous orientation polarization of the molecular dipoles during film formation.^{8,9,18} Depending on the ETL thickness, the hole injection voltage V_i can be shifted even to reverse bias. In these devices, the HTL is already flooded with holes at voltages below V_{bi} , which can be witnessed in the capacitance of the device. The capacitance is no longer the geometric value, $C_{geo} = \left(\frac{d_{HTL}}{\epsilon_0 \epsilon_{HTL}} + \frac{d_{ETL}}{\epsilon_0 \epsilon_{ETL}} \right)^{-1}$, but is enhanced to the value of the ETL alone, $C_{ETL} = \frac{\epsilon_0 \epsilon_{ETL}}{d_{ETL}}$, where d denotes the thicknesses and the ϵ is the relative dielectric permittivities of the respective layers, and where the capacitance per unit area is used. The hole injection voltage V_i giving the transition from the geometric to the ETL capacitance can be obtained from capacitance-voltage experiments, or displacement current measurements as shown in the [supplementary material](#).^{8,15,17}

If the capacitance is measured versus frequency at a bias $V_i < V < V_{bi}$, the transition from the geometric to the ETL capacitance occurs at a characteristic frequency f_i , as can be seen in the measurement of Fig. 2. This frequency is defined by the inflection point of the C-f plot, which is best derived as the minimum of the numerically computed first derivative. When the temperature is lowered, this transition occurs at lower frequency. The temperature dependent behaviour of the capacitance-frequency experiment (C-f-T), especially the one of this transition frequency, can be used to analyse the thermal activation of the hole current.^{19–24} The activation energy is obtained from an Arrhenius analysis, as shown in the inset of Fig. 2, by employing

$$f_i(T) = f_0 \cdot \exp\left(\frac{-E_{act}}{k_B T}\right). \quad (1)$$

For the measurement in Fig. 2, we obtain an activation energy of 0.53 eV. The behaviour of the transition frequency can be understood from a simple equivalent circuit model of

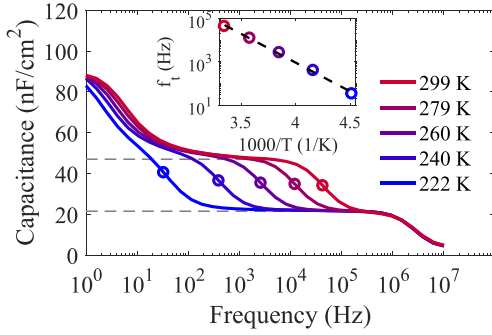


FIG. 2. Capacitance-frequency measurement at varied temperature for an α -NPD(77nm)/Alq₃(66nm) bilayer OLED at zero volts. The inset shows an Arrhenius plot of the temperature-dependent transition frequency which is marked by the symbols, giving an activation energy of 0.53 eV. The geometric capacitance and the higher ETL capacitance plateaus are also highlighted by the dashed grey lines.

the bilayer OLED, where the two layers are represented by RC elements [see Fig. 1(b)].^{8,24–26} When the conductance of the HTL increases with temperature, its resistance decreases. The transition frequency for the case that the HTL is significantly less resistive than the ETL is given by²⁷

$$f_t = \frac{1}{R_{HTL} \cdot (C_{HTL} + C_{ETL})}. \quad (2)$$

Thus, a HTL conductance increasing exponentially with increasing temperature corresponds to a resistance decreasing like $R_{HTL}(T) = R_0 \cdot \exp\left(\frac{E_{act}}{k_B T}\right)$. Then, the transition frequency, being inversely proportional to the HTL resistance, is Arrhenius-activated as Eq. (1).

As a side remark, we would like to note that the observed capacitance increase at very low frequencies in Fig. 2 is an effect of the lateral conductivity of the PEDOT:PSS layer.²⁷ This parasitic capacitance is not accounted for in the simple equivalent circuit model. Furthermore, the influence of an external series resistance of 80 Ω produces the capacitance decay at high frequencies above 1 MHz.

However, this simple model reveals that the activation energy of f_t contains contributions of both the hole injection barrier (E_{inj}) at the interface with the HIL and the thermal activation of the hole mobility inside the HTL (E_μ). To account for this increased complexity, we move to a microscopic description of the conductivity of the HTL, which allows us to describe and investigate the two processes independently. In a first approximation, we assume that the hole concentration in the HTL is constant and equal to the concentration at the HIL contact interface. Ensuring Fermi-level alignment at the HIL/HTL interface, the hole density in the HTL is given by $p_{HTL} = p_0 \cdot \exp\left(\frac{-E_{inj}}{k_B T}\right)$, where p_0 is the density-of-states of the HTL. The conductivity of the HTL is defined by $G_{HTL} = q \cdot p_{HTL} \cdot \mu_{HTL}$, with q being the unit charge and μ_{HTL} the hole mobility. If the mobility is thermally activated by E_μ , we obtain

$$\begin{aligned} G(T) &= q \cdot p_0 \cdot \exp\left(\frac{-E_{inj}}{k_B T}\right) \cdot \mu_0 \cdot \exp\left(\frac{-E_\mu}{k_B T}\right) \\ &= G_0 \cdot \exp\left(-\frac{E_{inj} + E_\mu}{k_B T}\right). \end{aligned} \quad (3)$$

The consequent assumption is that the observed temperature-dependence of G and therefore of the transition frequency is determined by the sum

$$E_{act} = E_{inj} + E_\mu. \quad (4)$$

These thoughts make it clear that the two parameters cannot be decoupled easily, if only C-f-T data are analysed. As we noted in a previous publication, measured C-f-T data could be fitted with a high injection barrier and temperature-independent mobility, thereby however leading to unrealistically high mobility values.¹⁷ Obviously a good fit would also be obtained by setting the injection barrier E_{inj} zero and putting all thermal activation into the mobility.

In summary, assuming that the hole concentration and therefore the conductivity in the HTL are constant already gives a qualitative understanding of the temperature dependence of the transition frequency. We will later see that it is, however, a too simplified model to quantitatively determine the activation energies.

In order to decouple the two activation energies, we propose to perform a second, independent experiment at different temperatures, namely MIS-CELIV. The CELIV technique is mostly employed to determine the charge carrier mobility from the characteristic drift time leading to a peak in the measured current.^{14,28,29} In our previous publication, we have demonstrated that this technique can be employed for mobility determination in the context of polar OLEDs,¹⁵ which behave like MIS-diodes in the accumulation regime for applied bias voltages between the hole injection voltage V_i and the built-in voltage V_{bi} . Under this condition, the CELIV current shows a peak on top of a constant displacement current and allows determination of the time for charge transit across the HTL, which is related to the charge-carrier mobility by^{15,28,30}

$$\mu = \frac{2d_{HTL}^2}{\mathcal{A} \cdot t_{tr}^2} \cdot \left(1 + \frac{\varepsilon_{HTL} d_{ETL}}{\varepsilon_{ETL} d_{HTL}}\right), \quad (5)$$

where ε denotes the relative dielectric permittivity and d is the thickness of the respective layers, $\mathcal{A} = dV/dt < 0$ is the applied voltage ramp, and t_{tr} is the transit time.

We have shown that this technique is best employed using offset voltages just above the hole injection voltage, thereby avoiding space-charge effects.¹⁵ In this limit, the transit time is equal to the transient position of the current peak.²⁸ Figure 3 shows the temperature-dependence of such a measurement, together with the Arrhenius plot of the extracted mobility from measurements at different offset voltages, thereby assuming a thermally activated mobility, in line with Eq. (3)^{31–34}

$$\mu(T) = \mu_0 \cdot \exp\left(\frac{-E_\mu}{k_B T}\right). \quad (6)$$

We determine a mobility activation energy of 0.22–0.28 eV, where the highest value is obtained for offset voltages just above the hole injection voltage and therefore the most reliable one. The infinite temperature extrapolation of the hole mobility in α -NPD given by the fit is $\mu_0 = 3.5 \text{ cm}^2/\text{V s}$.

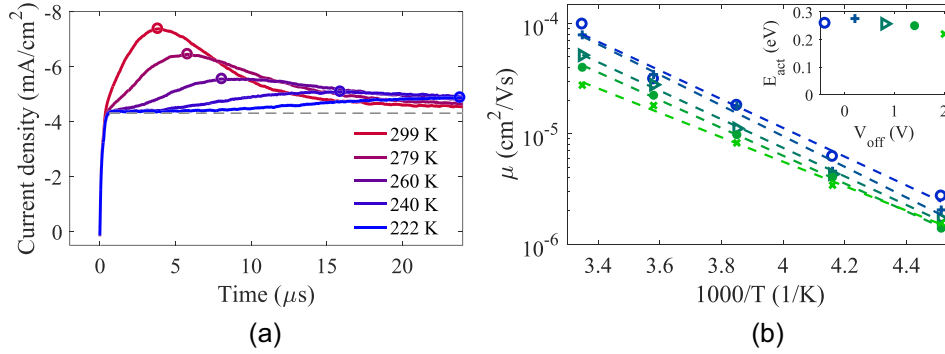


FIG. 3. MIS-CELIV measurement of an α -NPD(77 nm)/Alq₃(66 nm) bilayer OLED for varied temperature. The ramp rate is -0.2 V/ μ s, and the offset voltage prior to the ramp was varied. Left: Measured current vs time for an offset voltage of 0.2 V. The grey dashed line denotes the displacement current corresponding to the geometric capacitance and the symbols denote the transit time used to calculate the mobility. Right: Arrhenius plot and linear fits for the measurements at offset voltages from -0.4 to 2.0 V, denoted by different symbols. The inset shows the determined activation energies, lying between 0.22 eV and 0.28 eV.

For simplicity, we assume that the non-uniform electric field that may be present in the HTL does not affect the analysis and that the observed MIS-CELIV mobility is mainly influenced by the thermal activation and not the field-dependence. Since the MIS-CELIV experiments are carried out for the same electrical driving conditions (i.e., ramp rate), this seems a safe assumption.

As there is no energy barrier for charge extraction, the determined activation energy from the MIS-CELIV experiment is only the thermal activation of the hole mobility E_{μ} . Thus, by combining this experiment with the C-f-T technique we believe to be able to individually determine the two activation energies E_{inj} and E_{μ} .

IV. COMPARISON WITH DRIFT-DIFFUSION MODELLING

We aim to validate the proposed method by using a two-step approach. In the first “forward” simulation, we calculate the two device characterization signals, namely C-f-T and MIS-CELIV current transients at various temperatures. In the second step, the above analytical approach is applied to the two kinds of signals. The extracted parameters for temperature-dependent charge mobility and injection are compared to the model input parameters used in the “forward” simulations. This allows us to validate the self-consistency and how reliably we can obtain the activation energies by the combined experiments using basic analytical formulas.

The boundary condition in the injection model is that the Fermi-level at the contact is aligned. Then, an injection barrier between the HIL and HTL leads to a thermally activated exponential increase of the boundary charge density with temperature as

$$p(x=0) = p_0 \cdot \exp\left(\frac{-E_{inj}}{k_B T}\right). \quad (7)$$

This is the same boundary condition as stated above in the simplified model. However, we do no longer assume a constant charge density throughout the HTL, but the density profile is calculated self-consistently in the drift-diffusion

approach. Here, we do not take barrier lowering due to the image charge effect into account.

For the hole mobility in α -NPD, we use the above-mentioned temperature dependent model, Eq. (6), where we set the mobility at 300 K to a value of 10^{-4} $\text{cm}^2/\text{V s}$, which we determined from our CELIV measurements. Other model parameters have been chosen in accordance with measurements as well, and are summarized in the [supplementary material](#). We then systematically varied the hole injection barrier E_{inj} and the mobility activation energy E_{μ} , in order to investigate their influence on the validity of the analysis method.

Figure 4 shows two exemplary simulations ($E_{inj} = 0.4$ eV, $E_{\mu} = 0.2$ eV) of the C-f-T and temperature-dependent MIS-CELIV. We also mark the relevant transition frequencies and CELIV peaks, respectively, and show the Arrhenius-plots with the fits in the insets. The mobility in the CELIV simulations is determined using Eq. (5), as we perform simulations in the small-charge regime with offset voltages just above V_r .

For the C-f-T data, we expect that the extracted activation energy is the sum of both the injection barrier and hole mobility activation, while for the CELIV experiment we expect to find only the mobility activation. From the simulation data of Fig. 4, we extract a total activation energy of 0.51 eV from C-f-T and an activation energy of 0.18 eV from MIS-CELIV, compared to the expected values of 0.6 eV and 0.2 eV, respectively. Thus, for example, in Fig. 4, the error for determination of E_{μ} by the analytical method is only 0.02 eV, and the error of the total activation energy determined from C-f-T is 0.09 eV, leading to a total combined error for the injection barrier of 0.11 eV. We calculated this kind of systematic error for a large series of simulations performed by systematically varying both the hole injection barrier and the hole mobility activation energy. This deviation shown in Fig. 5 is therefore a measure of the uncertainty of the analysis method based on Eqs. (1), (3), and (6).

For the MIS-CELIV simulations analysed in Fig. 5(a), we find nearly constant deviations <0.07 eV for injection barriers below 0.25 eV. Here, our assumption that this experiment is insensitive to the injection barrier holds. However, for larger injection barriers there is an influence and the deviation increases up to 0.15 eV.

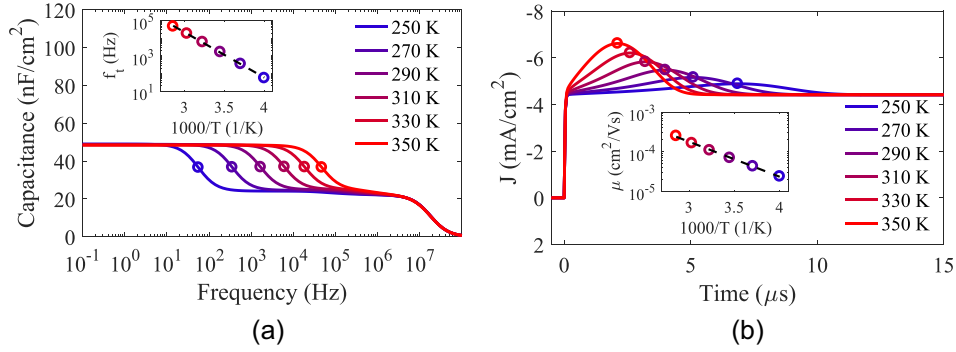


FIG. 4. Simulation of an α -NPD (80 nm)/Alq₃ (60 nm) bilayer device at varied temperature. The hole injection voltage is -1.2 V, injection barrier is 0.4 eV, and the thermal mobility activation energy is 0.2 eV. Left: Capacitance-frequency at zero applied bias. The inset shows an Arrhenius plot of the transition frequency, resulting in an activation energy of 0.51 eV. Right: MIS-CELIV currents for an offset voltage of -0.7 V and a ramp rate of -0.2 V/ μ s. The inset shows an Arrhenius plot of the mobilities determined by Eq. (5), resulting in an activation energy of 0.18 eV.

Figure 5(b) shows that for C-f-T the error in determining the activation energy is imposed by the injection barrier alone, while varying the mobility activation energy does not influence it. We find that the maximum deviation for determining the combined activation energy is 0.20 eV, at an injection barrier of 0.25 eV. Below this value, the error is on the same order of E_{act} , meaning that the experiment shows only the temperature dependence of the mobility, when the device is not contact-limited. This actually indicates that the mobility activation energy may also be obtained from C-f-T in the case of ideal ohmic contacts, with a very small systematic error below 100 meV. It is noteworthy that for injection barriers higher than 0.25 eV the error decreases and the uncertainty of the extracted parameter will become as low as 0.05 – 0.10 eV emphasizing that this is a powerful method to simultaneously estimate both activation energies.

We conclude that indeed the MIS-CELIV experiment is largely determined by the mobility activation energy. For small extracted E_{act} values, the mobility activation can then be reliably determined. This is good news as the mobility activation energy in organic materials usually lies in the range of 0.1 – 0.3 eV.^{23,35} Thus from the MIS-CELIV alone this parameter can be determined.

In the [supplementary material](#), we show the data of Fig. 5 in a different representation. This also clarifies that for very good contacts the mobility activation energy may be determined well from the CELIV experiment. On the other hand, for very high total activation energies observed in the C-f-T

the error from the CELIV experiment will impose on the injection barrier, so that the decoupling is more difficult. This means that the injection barrier cannot be determined as reliably as the mobility activation using the analytical approach. Furthermore, as the deviation from the real value is always positive, the extracted parameters always underestimate the true values and thus give a quantitative lower limit.

For a better understanding of the systematic error on parameter extraction, we show the simulated equilibrium charge carrier density and electric field profiles for varied injection barriers in Fig. 6. These profiles do not depend on the choice of mobility or mobility activation, as they depict the thermodynamic equilibrium. This is also the reason why the mobility activation does not influence the error in Fig. 5(b).

As shown in Fig. 6(b), for high injection barriers the holes accumulate only at the internal interface with the ETL, while for low barriers there is a considerable amount of charge also at the interface with the HIL, and in the bulk. Therefore, the analytical approach of Eq. (3) assuming position-independent density and field turns out to be too simplified. It seems that for non-limiting contacts the assumption of a homogeneous conductivity is better fulfilled, leading to the small errors in parameter determination.

In order to trust a maximum error of 0.25 eV, we performed further simulations where other modelling parameters were varied. For these simulations, we set $E_{inj} = 0.4$ eV and $E_{\mu} = 0.2$ eV, so we would expect activation energies to lie at 0.6 eV and 0.2 eV for C-f-T and CELIV, respectively. We observe that the parameter extraction is not affected by

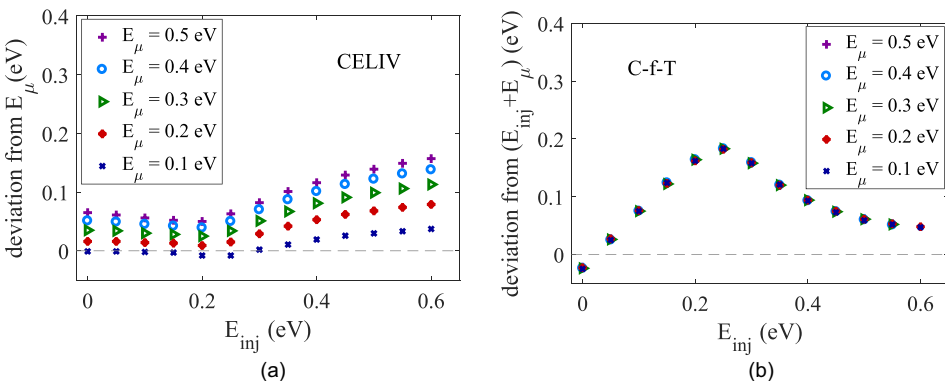


FIG. 5. Analysis of the accuracy of extracted activation energies. The plots show the difference between the theoretical value (=simulation input parameter) and the analysed value of the activation energy, for varied injection barrier E_{inj} and at different values of mobility activation E_{μ} . Left: Deviation for MIS-CELIV with a ramp of -0.2 V/ μ s and an offset voltage of -1.5 V, the theoretical value is $E_{act} = E_{\mu}$. Right: Deviation for capacitance-frequency at 0 V, the theoretical value is $E_{act} = E_{inj} + E_{\mu}$.

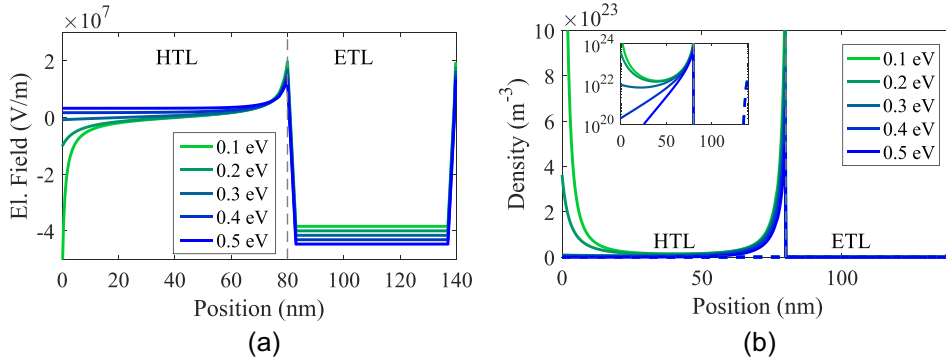


FIG. 6. Simulated electric field and charge carrier density profiles in the bilayer at thermal equilibrium, for varied injection barriers. Left: Electric field profile at $V=0$ and $T=300$ K. Right: Equilibrium charge density profile at $V=0$ and $T=300$ K, holes are denoted by solid lines, electrons by dashed lines.

the electron mobility in the ETL, the electron injection barrier at the cathode, or the internal energy barrier for holes between the HTL and ETL. The C-f-T analysis is further independent of the density of states (DOS) in the HTL and the mobility prefactor μ_0 for holes. This shows the robustness of the method and allows us to specify 0.25 eV as an upper limit of the systematic error. It also confirms our initial assumption that the combination of the two experiments is indeed suited to disentangle the two activation energies.

We further find that for C-f-T the offset voltage plays only a minor role, so the working point (between V_i and V_{bi} , naturally) does not matter. Concerning the activation energy of the mobility using the MIS-CELIV experiment, it turns out that an offset voltage just above the hole injection voltage (-2 V in our case) leads to the most accurate results. Part of this error probably stems from the evaluation of the mobility by Eq. (5), where for larger peaks the transit time has to be defined differently.^{28,30} Finally, also the voltage ramp was varied, and we find the smallest deviation from the input model parameter for high voltage ramps in the range of -1 V/ μ s. Thus, by using appropriate measurement conditions the uncertainty of the extracted parameters can be narrowed further. The results from these additional parameter variations can be found in the [supplementary material](#).

V. DISCUSSION

As we have seen, the implicit assumption of constant charge and field profiles throughout the layer employed in the analytical model gives rise to the systematic errors in parameter determination. A first improvement of this situation would be the use of a more complex analytical model taking the inhomogeneous density into account.³⁶ In order to further narrow down the confidence interval of the parameters, a full drift-diffusion modelling and global fitting of the measurement data is conceivable, and we have already demonstrated such a procedure before.^{37,38} However, even though the analytical description is not powerful enough to get a very accurate value of the injection barrier, we believe that this method still can be useful to compare different devices or to monitor the degradation of one device.

Overall, it seems that we can determine E_μ very well, while we systematically underestimate E_{act} from C-f-T, because the “effective” injection barrier is about 0.1–0.2 eV smaller than the nominal value.

This approach is not limited to bilayer OLEDs, as we have only exploited their behaviour as MIS-diodes here. Conventional MIS-devices comprising an insulating layer will obviously also work. An exemplary simulation of the field and density profiles in a MIS-device can be found in the [Supplementary material](#). The profiles are qualitatively identical; thus, the analytical procedure is as valid as in the polar OLED case. As a side note we want to mention that the thickness ratios in standard MIS-devices are usually different from the bilayer OLEDs, and therefore, the CELIV mobility is often analysed in the saturation regime, demanding a correction factor for the determination of t_{tr} in Eq. (5).^{15,28,30}

Therefore, the method presented may be applied generally to new organic materials. In different bilayer stack layouts comprising a polar layer,^{15,39} or in dedicated MIS devices it would then also be possible to gain information on the electron mobility and its thermal activation. In multilayer OLED stacks, the approach may also be useful to assess the effective properties of carriers injected and transported to the emission layer.

The value obtained here for the mobility activation in α -NPD is 0.28 eV. In organic materials exhibiting disordered transport, this effective activation energy depends on the shape of the density of states (DOS). In the context of the field- and temperature-dependent extended Gaussian disorder and correlated Gaussian disorder models (EGDM and ECDM), the width of the density of states σ can be related to the transport activation by $E_\mu = \frac{4}{9} \frac{\sigma^2}{k_B T}$.^{40,41} With this formula and the activation energy of $E_\mu = 0.28$ eV, we obtain a DOS width of $\sigma = 125$ meV at 300 K, in good agreement with values reported earlier for α -NPD.^{42–44} Concerning the temperature activation itself, the disorder models usually note a $1/T^2$ dependence instead of the observed and discussed $1/T$ behaviour.^{45–47} In fact, at high temperatures (>200 K) the two dependencies cannot unambiguously be distinguished, and the disorder models are fully consistent with Arrhenius activation.^{35,48,49}

The energetic barrier for charge injection is most relevant for efficient OLEDs with a low turn-on voltage. The experimental finding that small injection barriers (<0.2 eV) are not “seen” by the charges is confirmed by the simulation, without special care for the interface modelling. Thus, if the device is not contact-limited the mobility activation energy will be the only factor contributing to E_{act} determined from C-f-T. For such small barriers, the chosen contact model assuming Fermi-level alignment is physically more

meaningful than the thermionic emission or tunnelling models, which are valid rather for high energetic barriers.^{50,51} Including barrier lowering effects has not been in the scope of this work, but we encourage to investigate this refinement as well as the influence of a Gaussian DOS on injection further.

Even though there are several formulations for injection and mobility models, it remains an experimental challenge to discriminate one from the other. Therefore, we concentrate on the determination of effective material parameters. Concerning the mobility temperature activation, this has been most often investigated in unipolar devices by experimental techniques such as space-charge limited current,^{42,52} time-of-flight,⁵³ or negative differential susceptance.⁵⁴ However, as we have shown above, the current is always dependent on both the mobility activation and the injection barrier. So good care must be taken when fabricating unipolar devices and analysing these measurements. Alternatively, as proposed here, extraction experiments like CELIV are much less sensitive to the injection barrier, and therefore better suited.

Concerning the injection barrier between two organic semiconducting materials, that is the energy level offset between their conduction bands, its experimental assessment is even more problematic. The most common techniques to analyse the valence and conduction bands of organic materials as well as the workfunctions of metals are photoelectron spectroscopy and Kelvin probe.^{55–57} In order to determine the energy offset between two materials, a series of devices need to be fabricated and measured, where the second layer is deposited onto the first with varied thickness, therefore allowing to probe the position-dependent energetics (band-bending).^{58–61} While these techniques have proven valid and reproducible, they are expensive and time-consuming, and multiple devices are needed. Furthermore, these techniques also have their systematic errors for parameter determination; for UPS errors in the range of 0.1–0.35 eV have been reported for organic materials.^{61–65}

Another approach seen in the literature is the use of IV-curves and capacitance-voltage measurements for the extraction of injection barriers.^{40,66,67} However, as mentioned before, injection currents always depend on both the barrier and the mobility, so in these cases probably an effective total activation is observed. Furthermore, usually simplified layer stacks have to be used.

We believe that temperature-dependent electrical measurements on MIS-devices or complete polar OLEDs can be more practical and relevant. The method presented in this work can be performed on complete layer stacks, and results are obtained more quickly and with less consumption of resources. And apart from the parameters discussed in this text, the temperature-dependence of OLEDs and OSCs is by itself an important experiment on the way of device optimization.

VI. SUMMARY

We have presented an approach how to decouple the different activation energies for hole transport and injection in polar bilayer OLEDs. For this purpose, we combine C-f-T

data with temperature-dependent MIS-CELIV measurements. From a first simple analytical model, it becomes clear that the C-f-T data contain contributions of both the temperature dependent charge injection and hole mobility. Using a self-consistency analysis enabled by numerical drift-diffusion simulation we determine the accuracy of the extracted parameters depending on the model input values of the injection barrier and mobility activation energy. In this analysis, we find that the extracted values are always lower than the true model parameters by up to 0.2 eV. The main reason for the deviation is the highly inhomogeneous charge profile in the hole transport layer leading to a non-constant conductivity, and the fact that barriers below 0.2 eV do not limit charge injection, which is not taken into account in the analytical expression.

We applied this method to a prototypical bilayer OLED, based on the hole transport layer α -NPD and the polar ETL Alq₃, and employing the hole injection layer PEDOT:PSS. We deduced the hole mobility activation energy in α -NPD to be 0.28 [+0.1; –0.0] eV, which can be translated into a width of the gaussian density of states of 125 meV, in good accordance with previous reports in the literature. The effective injection barrier from PEDOT:PSS into α -NPD is found to be 0.25 [+0.2; –0.0] eV.

The presented approach can be applied in a general manner to determine the activation energies of new materials used as injection or active layers. MIS-devices, consisting either of a bilayer with a polar material or comprising a fully insulating layer, in conjunction with temperature-dependent experiments, therefore represent a highly valuable approach for parameter determination.

SUPPLEMENTARY MATERIAL

See [supplementary material](#) for C-V and CELIV schematics, further simulation results on polar bilayers, and field and density profiles in MIS-devices.

ACKNOWLEDGMENTS

We acknowledge financial support from the Swiss Natl. Science Foundation (SNSF; Project No. 151563) and the Deutsche Forschungsgemeinschaft (DFG; Contract No. BR 1728/15-1) within the CARDYN project.

¹E. Knapp and B. Ruhstaller, *J. Appl. Phys.* **117**, 135501 (2015).

²E. Knapp and B. Ruhstaller, *Proc. SPIE* **9566**, 95660X (2015).

³Z. Kohári, E. Kollár, L. Pohl, and A. Poppe, *Microelectron. J.* **44**, 1011 (2013).

⁴J. Park, J. Lee, and Y.-Y. Noh, *Org. Electron.* **13**, 184 (2012).

⁵American Society for Testing Materials, ASTM G173-03(2012), Standard Tables for Reference Solar Spectral Irradiances: Direct Normal and Hemispherical on 37° Tilted Surface, 2012.

⁶Q. Burlingame, G. Zanotti, L. Ciannaruchi, E. A. Katz, and S. R. Forrest, *Org. Electron.* **41**, 274 (2017).

⁷N. Bristow and J. Kettle, *J. Renewable Sustainable Energy* **7**, 013111 (2015).

⁸W. Brütting, S. Berleb, and A. G. Mückl, *Org. Electron.* **2**, 1 (2001).

⁹Y. Noguchi, Y. Miyazaki, Y. Tanaka, N. Sato, Y. Nakayama, T. D. Schmidt, W. Brütting, and H. Ishii, *J. Appl. Phys.* **111**, 114508 (2012).

¹⁰T. D. Schmidt, L. Jäger, Y. Noguchi, H. Ishii, and W. Brütting, *J. Appl. Phys.* **117**, 215502 (2015).

¹¹S. Braun, W. R. Salaneck, and M. Fahlman, *Adv. Mater.* **21**, 1450 (2009).

¹²A. Kanwat and J. Jang, *RSC Adv.* **6**, 114800 (2016).

- ¹³See www.fluxim.com for “Platform for All-In-One characterisation of Solar Cells, Fluxim AG” (2017).
- ¹⁴G. Juška, K. Arlauskas, M. Viliūnas, and J. Kočka, *Phys. Rev. Lett.* **84**, 4946 (2000).
- ¹⁵S. Züfle, S. Altazin, A. Hofmann, L. Jäger, M. T. Neukom, T. D. Schmidt, W. Brütting, and B. Ruhstaller, *J. Appl. Phys.* **121**, 175501 (2017).
- ¹⁶See www.fluxim.com for “Setfos 4.4, Fluxim AG” (2017).
- ¹⁷S. Altazin, S. Züfle, E. Knapp, C. Kirsch, T. Schmidt, L. Jäger, Y. Noguchi, W. Brütting, and B. Ruhstaller, *Org. Electron.* **39**, 244 (2016).
- ¹⁸S. Berleb, W. Brütting, and G. Paasch, *Org. Electron.* **1**, 41 (2000).
- ¹⁹J. Scherbel, P. H. Nguyen, G. Paasch, W. Brütting, and M. Schwoerer, *J. Appl. Phys.* **83**, 5045 (1998).
- ²⁰O. Armbruster, C. Lungenschmied, and S. Bauer, *Phys. Rev. B* **86**, 235201 (2012).
- ²¹T. Kobayashi, Z. J. L. Kao, and T. Nakada, *Sol. Energy Mater. Sol. Cells* **143**, 159 (2015).
- ²²J. Ahn, T. W. Kim, and W. J. Lee, *J. Ceram. Process. Res.* **13**, 163 (2012).
- ²³F. Reis, D. Mencaraglia, S. Oould Saad, I. Séguy, M. Oukachmih, P. Jolinat, and P. Destruel, *Synth. Met.* **138**, 33 (2003).
- ²⁴S. Berleb, “Raumladungsbegrenzte Ströme und Hoppingtransport in organischen Leuchtdioden aus Tris(8-hydroxyquinolin)-Aluminium (Alq3),” Ph.D. thesis (Universität Bayreuth, Bayreuth, 2001).
- ²⁵S. Nowy, “Understanding losses in OLEDs: Optical device simulation and electrical characterization using impedance spectroscopy,” Ph.D. thesis (Universität Augsburg, Augsburg, 2010).
- ²⁶S. Nowy, W. Ren, J. Wagner, J. A. Weber, and W. Brütting, *Proc. SPIE* **7415**, 74150G (2009).
- ²⁷S. Nowy, W. Ren, A. Elschner, W. Lövenich, and W. Brütting, *J. Appl. Phys.* **107**, 054501 (2010).
- ²⁸G. Juška, N. Nekrašas, and K. Genevicius, *J. Non-Cryst. Solids* **358**, 748 (2012).
- ²⁹A. Armin, G. Juska, M. Ullah, M. Velusamy, P. L. Burn, P. Meredith, and A. Pivrikas, *Adv. Energy Mater.* **4**, 1300954 (2014).
- ³⁰J. Važgėla, K. Genevicius, and G. Juška, *Chem. Phys.* **478**, 126 (2016).
- ³¹W. D. Gill, *J. Appl. Phys.* **43**, 5033 (1972).
- ³²L. Bozano, S. A. Carter, J. C. Scott, G. G. Malliaras, and P. J. Brock, *Appl. Phys. Lett.* **74**, 1132 (1999).
- ³³P. Servati, A. Nathan, and G. A. J. Amaratunga, *Phys. Rev. B* **74**, 245210 (2006).
- ³⁴P. W. M. Blom, M. J. M. de Jong, and M. G. van Munster, *Phys. Rev. B* **55**, R656 (1997).
- ³⁵N. I. Craciun, J. Wildeman, and P. W. M. Blom, *Phys. Rev. Lett.* **100**, 056601 (2008).
- ³⁶S. Altazin, R. Clerc, R. Gwoziecki, D. Boudinet, G. Ghibaud, G. Pananakakis, I. Chartier, and R. Coppard, *Org. Electron.* **12**, 897 (2011).
- ³⁷M. Neukom, S. Züfle, and B. Ruhstaller, *Org. Electron.* **13**, 2910 (2012).
- ³⁸S. Züfle, M. T. Neukom, S. Altazin, M. Zinggeler, M. Chrapa, T. Offermans, and B. Ruhstaller, *Adv. Energy Mater.* **5**, 1500835 (2015).
- ³⁹L. Jäger, T. D. Schmidt, and W. Brütting, *AIP Adv.* **6**, 095220 (2016).
- ⁴⁰T. van Woudenberg, “Charge injection into organic semiconductors,” Ph.D. thesis (Rijksuniversiteit Groningen, Groningen, 2005).
- ⁴¹V. Arkhipov, E. Emelianova, G. Adriaenssens, and H. Bässler, *J. Non-Cryst. Solids* **299–302**, 1047 (2002).
- ⁴²R. Rohloff, N. B. Kotadiya, N. I. Crăciun, P. W. M. Blom, and G. A. H. Wetzelaer, *Appl. Phys. Lett.* **110**, 073301 (2017).
- ⁴³K. L. Tong, S. W. Tsang, K. K. Tsung, S. C. Tse, and S. K. So, *J. Appl. Phys.* **102**, 093705 (2007).
- ⁴⁴T. Y. Chu and O. K. Song, *J. Appl. Phys.* **104**, 023711 (2008).
- ⁴⁵W. F. Pasveer, P. A. Bobbert, and M. A. J. Michels, *Phys. Status Solidi C* **1**, 164 (2004).
- ⁴⁶S. Novikov and A. Vannikov, *Chem. Phys.* **169**, 21 (1993).
- ⁴⁷H. Bässler, *Phys. Status Solidi B* **175**, 15 (1993).
- ⁴⁸R. Coehoorn, W. F. Pasveer, P. A. Bobbert, and M. A. J. Michels, *Phys. Rev. B* **72**, 155206 (2005).
- ⁴⁹S. van Mensfoort, “Effects of disorder on the charge transport and recombination in organic light-emitting diodes,” Ph.D. thesis (Technische Universiteit Eindhoven, Eindhoven, 2009).
- ⁵⁰G. G. Malliaras and J. C. Scott, *J. Appl. Phys.* **85**, 7426 (1999).
- ⁵¹G. G. Malliaras and J. C. Scott, *J. Appl. Phys.* **83**, 5399 (1998).
- ⁵²W. Brütting, S. Berleb, and A. Mückl, *Synth. Met.* **122**, 99 (2001).
- ⁵³P. Borsenberger, E. Magin, and J. Shi, *Phys. B: Condens. Matter* **217**, 212 (1996).
- ⁵⁴T. Okachi, T. Nagase, T. Kobayashi, and H. Naito, *Thin Solid Films* **517**, 1331 (2008).
- ⁵⁵I. G. Hill and A. Kahn, *J. Appl. Phys.* **84**, 5583 (1998).
- ⁵⁶I. G. Hill, D. Milliron, J. Schwartz, and A. Kahn, *Appl. Surf. Sci.* **166**, 354 (2000).
- ⁵⁷H. Ishii, K. Sugiyama, E. Ito, and K. Seki, *Adv. Mater.* **11**, 605 (1999).
- ⁵⁸J. Hwang, A. Wan, and A. Kahn, *Mater. Sci. Eng., R* **64**, 1 (2009).
- ⁵⁹N. Koch, A. Kahn, J. Ghijsen, J.-J. Pireaux, J. Schwartz, R. L. Johnson, and A. Elschner, *Appl. Phys. Lett.* **82**, 70 (2003).
- ⁶⁰S. L. M. van Mensfoort, V. Shabro, R. J. de Vries, R. A. J. Janssen, and R. Coehoorn, *J. Appl. Phys.* **107**, 113710 (2010).
- ⁶¹A. Rajagopal, C. I. Wu, and A. Kahn, *J. Appl. Phys.* **83**, 2649 (1998).
- ⁶²J. D. Anderson, E. M. McDonald, P. A. Lee, M. L. Anderson, E. L. Ritchie, H. K. Hall, T. Hopkins, E. A. Mash, J. Wang, A. Padias, S. Thayumanavan, S. Barlow, S. R. Marder, G. E. Jabbour, S. Shaheen, B. Kippelen, N. Peyghambarian, R. M. Wightman, and N. R. Armstrong, *J. Am. Chem. Soc.* **120**, 9646 (1998).
- ⁶³P. I. Djurovich, E. I. Mayo, S. R. Forrest, and M. E. Thompson, *Org. Electron.* **10**, 515 (2009).
- ⁶⁴Y. Gao, *Mater. Sci. Eng., R* **68**, 39 (2010).
- ⁶⁵T. Chassé, C.-I. Wu, I. G. Hill, and A. Kahn, *J. Appl. Phys.* **85**, 6589 (1999).
- ⁶⁶S. L. M. van Mensfoort and R. Coehoorn, *Phys. Rev. Lett.* **100**, 086802 (2008).
- ⁶⁷Z. Wang, Y. Lou, S. Naka, and H. Okada, *Chem. Phys. Lett.* **501**, 75 (2010).